Realization of the Control Software of the Rheometer for Viscoelastic Tests on Articular Cartilage

Guido Giuseppe Garozzo
University of Catania
Department of Elettics, Elettronics and Informatics Engineering
Viale A.Doria 6, 95125, Catania, Italy
Email: guido.garozzo@studium.unict.it

***Abstract*—The Control software developed in LabVIEW was realized for an instrument for the measurement of viscoelastic parameters of the articular cartilage in a humid environment, in particular, for the measurement of the complex modulus G and the loss coefficient tanδ, as a function of the frequency and the applied pressure. The rheometer is capable of applying a controlled displacement of between 10% and 30% of the height of the same sample, and a rotation on the plane of the specimen of 5 to 15 degree in a frequency range of 0.01 Hz and 2 Hz. The tests were carried out initially on semifluid silicone specimens, to test and calibrate the equipment; then, on specimens of cartilage and sub-chondral bone immersed in saline solution. The tests carried out have shown the module and phase values of G in good agreement with those found in the literature, proving the effectiveness of the software by reducing the measurement error at the lowest possible.**

Keywords: Rheomoter, Articular Cartilage, LabVIEW, Viscoelastic, Complex Modulus

I. Introduction

The study of the viscoelastic properties arises from the need to derive the dynamic behavior of certain materials; for this purpose we use instruments named Rheometers. These instruments were born to study viscous or non-Newtonian fluids. Today, however, it also makes great use to characterize the viscoelastic properties of synthetic and biological materials [1]–[5]. Generally, a rheometric test consists in measuring a dynamic variable (force, torque, pressure) and a kinematic variable (velocity, displacement). There are various types of rheometers that can be classified according to the motion typology. These may be in rotational flow (closed trajectory) or in a non- rotational flow (open trajectory). The motion can occur by sliding between two surfaces, which can be in parallel planes, coaxial cylinders, cone-plate, parallel plates. The easiest way to study a material with a rheometer is to allow the fluid to move according to trajectories closed, ie repeated indefinitely in time. This principle is realized in the rotational rheometers. These can be stress-controlled, where the torque it imposed and the rotation is measured, or strain-controlled, where the rotation it imposed and the torque is measured. The functional principle of rotational rheometers consists in rotating a plate at a given speed, by a motor, to apply the rotational movement to specimen among the two plates. From the measurement of the torque can be gained the tension of the specimen and the speed of the applied shear gradient. In parallel- plates rheometers the shear gradient

$$\dot{\gamma} = \frac{\Omega r}{h} \tag{1}$$

varies with the radius. The torque can be written in terms of the shear stress integral:

$$\begin{aligned} M &= \int_0^R \sigma r(2\pi r)dr = \int_0^R \eta\dot{\gamma} r(2\pi r)dr \\ &= \frac{2\pi\Omega\eta}{h}\int_0^R r^3 dr = \frac{\pi\Omega\eta R^4}{2h} \end{aligned} \tag{2}$$

from which one can derive the equation of rheometer:

$$\eta = \frac{2Mh}{\pi R^4 \Omega} \tag{3}$$

For the simplicity of use, the parallel-plates rheometers are widely used to do measurement of viscoelastic properties. Aim of this work is to realize a low cost parallel-plates strain-controlled rheometer to measure the parameters of articular cartilage [6]–[8]. The cartilage is a particular type of connective tissue characterized by resistance and elasticity. It plays a role of structural support within the body and its composed of cells dispersed in an abundant extracellular matrix, rich in fiber and amorphous substance of protein origin. The articular cartilage is a layer of low friction bearing soft tissue that overlaps the articular bone ends in the junctions [9]–[12]. The ability of articular cartilage to withstand high compressive loads without being damaged is due to the multiphase nature of the tissue. The particular composition of the articular cartilage (AC) gives to it the viscoelastic properties, in fact the we can distinguish three phases: a "Solid phase" composed mainly of collagen fibers and macromolecules of PG tied to chains of hyaluronic acid; a "Fluid phase" mainly composed of water; an "Ionic phase" composed of electrolytes dissolved in water with both negative and positive charge. These three phases act

together to create a tissue capable of bearing huge compression stress and the associated shear. The interstitial fluids of the AC are composed from the fluid and ionic phase. The AC is presented as a layered structure with three layer [5], [13]:

- Superficial Layer: with the major quantities of water and collagen's fibrils;
- Middle Layer: with quantities of water and collagen's fibrils less than the superficial layer;
- Deep layer: divided in two zones (Deep zone and Calcified zone) where quantities of water and collagen's fibrils are constant and the PG have the maximum concentration.

II. Design and creation of the Rheometer

To determine the dynamic viscoelastic response must submit the specimen to a condition of deformation that does not involve a change in volume nor a shift of interstitial fluid [10]. By applying a sinusoidal torque $M_t(t)$, the specimen will respond with a sinusoidal angular deformation γ but with a delay δ,

$$\begin{cases} M_t(t) = M_t \sin(\omega t) \Rightarrow \tau = \tau_0 \sin(\omega t) \\ \epsilon(t) = \epsilon \sin(\omega t + \delta) \Rightarrow \gamma = \gamma_0 \sin(\omega t + \delta) \end{cases} \quad (4)$$

where τ is the shear stress. The dynamic shear modulus or complex modulus G^* is defined by:

$$\frac{\tau}{\gamma} = G^* = G' + iG" = \left(\frac{\tau_0}{\gamma_0}\right)(\cos(\delta) - i\sin(\delta)) \quad (5)$$

$$|G^*| = \left(\frac{\tau_0}{\gamma_0}\right) \quad (6)$$

with the elastic modulus G' and the viscous modulus G".

To achieve the goal of measuring the viscoelastic properties, the measurement was made at different frequencies with a rotational rheometer made in lab. The design of the rheometer was done with the software $SolidWorks^{tm}$ (Fig. 1a). This rheometer is divided in two parts: an Upper part with the actuator and the load cell and a Bottom part with the stepper motor and the test chamber.

The rheometer was built following the design (Fig. 1b), and to keep the correct operation of the machine it was necessary to create the joints with bearings specifically for that purpose. The equipment is constituted of a metal frame with two crossbars. The upper part is connected the specimen compression system, in series to the load cell and to the upper compression plate. The lower crossbar supports, instead, the system of rotation, connected to the lower plate. The plates, together with the simple, are immersed in a plastic can, which contains a physiological solution, to performing the tests on the cartilage in a humid environment. A Robot-Italy 39BYGL bipolar stepper motor, equipped with endless screw to convert the rotary motion in a linear one, provides the vertical compression. For applying the torque has been used a bipolar stepper motor Phidgets 3321-0-28STH32 NEMA-11 with integrated planetary gearbox (Gearbox 27:1). It has a maximum speed of 120 rpm and a nominal torque of 1.4 Nm [14], [15]. The stepper motor is connected to a controller 1067-0 Phidgets Stepper Bipolar Phidget-HC, which allows you to control its position, velocity and acceleration. For measuring of the force, a load cell Laumas 150 N was used, with a NI DAQ 6008 acquisition card as a signal amplifier and a further signal amplifier (Transducer Techniques BMT-01). The stepper motor and the actuator are connected to the controller and this, through the USB port, to the control and processing system. The rheometer is made of a frame of metal sections, anchored to a base on which have been fixed the motor control board, the acquisition card and the signal amplifier. A custom-made threaded joint transmits the rotate motion to the cartilage. A vessel contains the cork lower disc, the cartilage and the saline solution for moist tests. On the upper crossbar was made a guide (with steel laminations and a bearing SKF [16]) for the load cell, in order to translate it vertically. An upper compression plate was installed under the load cell. This consist of an assembly of screw- bearing-cork's plate. The last has truncated cone shape. This system has two functions: to transmit the vertical load of the linear actuator for compressing, and sending the response of the simple to the torsion measurement system. The upper cork's plate, in fact, was vertically carved on one side to accommodate a very thin (0.5 mm) and flexible plate of plastic material (Plasticard). This is made with strain gauge (Fig. 2). The stepper motor and the actuator used, both have a step- by-step technology and have the same electrical characteristics, therefore, it was chosen a single controller with a sensitivity of 1/16 step, which activates one or other by means of a switch. A computer, with a software developed in NI LabVIEW, has allowed operating the machine and elaborating its measurements. A simulation software was created for laying the foundations to what later will be the final software. In this was considered the lower disc in the form of sine wave generator and the sample as a simple band pass filter, since the viscoelastic behavior has a frequency response similar.

III. Software implementation

The rheometer is controlled from a notebook with the control software (CS) created in the development environment NI $LabVIEW^{tm}$. The CS enables to make the measures totally automated. The peripherals needed to execute this task are: the NI DAQ 6009 used to read data from the load cell; a NI SCXI Chassis with NI SCXI 1520 plug-in to read the strain gauge data. At first, the CS applies compression to the specimen with the actuator and, after reaching a given force, the stepper start to impose the sinusoidal angular deformation. The shear stress was measured by a custom-made load cell with a strain gauge mounted on the Plasticard lamina [14], [17], [18]. Moreover, the software processes the measured data, calculates complex modulus and loss coefficient and ends with the construction of graphs and charts and exporting them in .xlsx file ($Excel^{tm}$). The front panel of the CS is divided in sheets; the first one is active at the beginning of the measure process until the compression applied to the specimen ends (Fig. 3). In this sheet is written the description of the measure. The second sheet, active in the oscillation phase of the measure

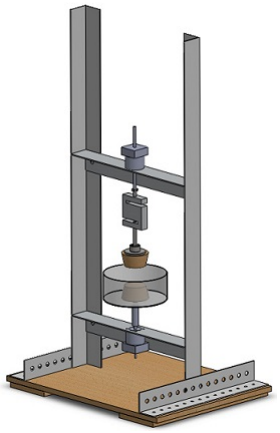

(a) Design

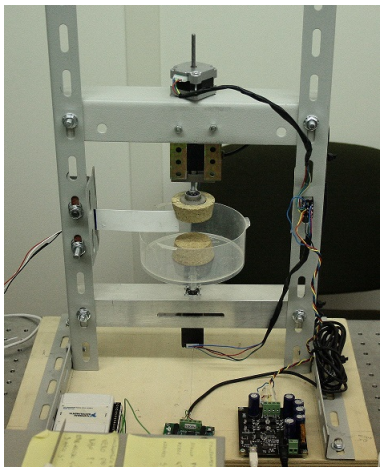

(b) Realization

Fig. 1. Design and realization of the Rheometer.

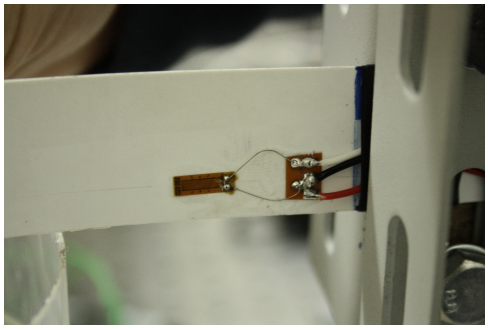

Fig. 2. Plastic lamina in the instrument

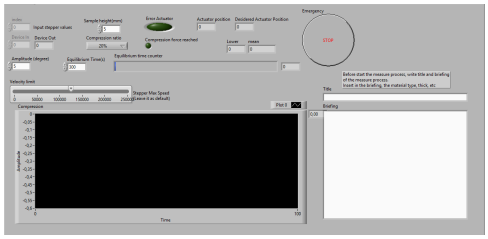

Fig. 3. Starting phase sheet

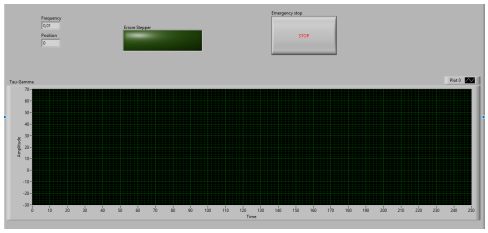

Fig. 4. Oscillation phase sheet

process, monitors the oscillations applied to the sample and its step-by-step response (Fig. 4). The others sheets contain the graphs of the viscoelastic properties of the sample, and

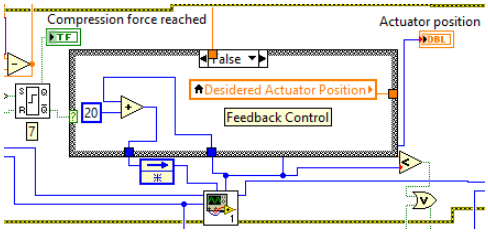

Fig. 5. Feedback control

the error indicators. The first step of the measure process consists to apply compression of the specimen until reaching the desired force. The actuator moves quickly and, when reaches the sample, the speed is reduced to avoid their over-compression. The compression is a function of the percentage of the height of the simple, which is to be compressed. In practice, in the instant in which it touches the specimen is applied the percentage of displacement defined. When the compression is finished, the CS stand by for the equilibrium time of the simple, usually 300 600 s . At the same time, the software evaluates the error due to interferences in the strain measurement system. A flip-flop custom-made in LabVIEW is used to record the instant of time that the actuator touches the simple, connecting the stepper driver to the load cell in closed loop with a feedback control (Fig. 5).

The second step of the measure process is the heart of the CS, this one imposes the oscillations to the specimen. The number of oscillation per frequency are usually 5 or 10 because is needed have the necessary raw data to be processed. In the last step the acquired Raw data are processed to extract the necessary information to our purpose. This process is needed to calculate the complex modulus and the loss coefficient of the tested material (Fig. 6) . The complex modulus is calculated with the equation 6 using labVIEW's blocks (Fig. 7) and the Loss coefficient is calculated with an algorithm that uses the Hilbert transform and other LabVIEW's blocks

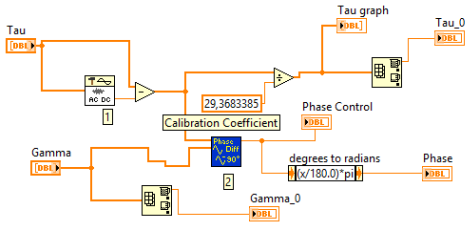

Fig. 6. Data processing block

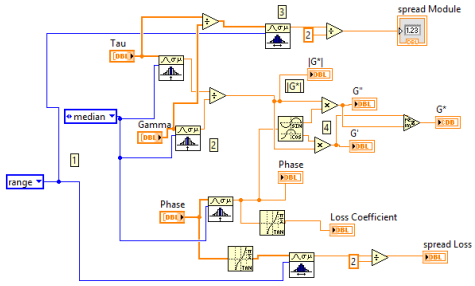

Fig. 7. Complex modulus algorithm

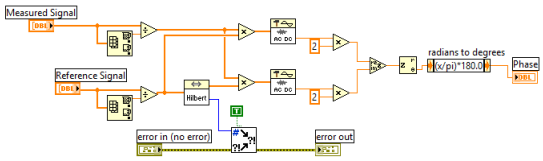

Fig. 8. δ extraction algorithm in labVIEW

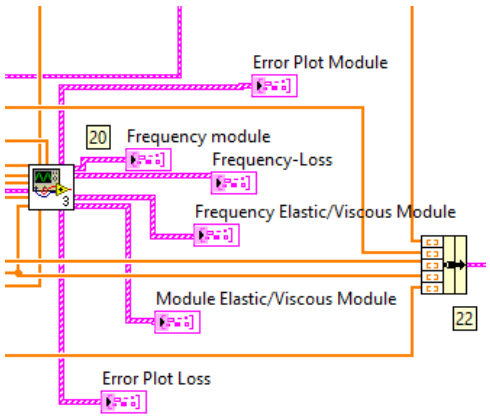

Fig. 9. Build Graphs block

to extract the phase delay δ (Fig. 8).

In the CS is present the function that allows to record the numeric data of the complex modulus and the loss coefficient, and their plots in the same file with the fitting's informations, such as fitting curve and polynomial equations (Fig. 9). The final data are plotted and recorded, in file .xlsx building a report file in the CS (Fig. 10).

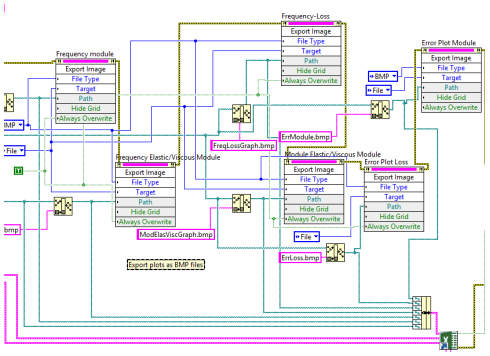

Fig. 10. Exports graphs sample

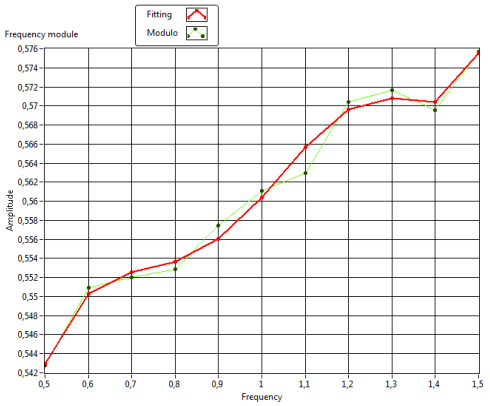

Fig. 11. Silicone Complex Modulus graph

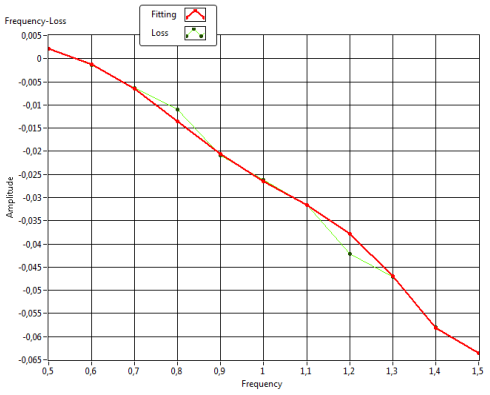

Fig. 12. Silicone Loss Coefficient graph

IV. Discussions and test's Results

Specimens of silicone were used to verify the functionality of the instrument and during its testing. Figure 11 shows the graph of the silicone module —G *—; the variation of the module is of the order of centimes of MPa, the resulting curve fitting has as equation:

$$f(x) = 0.425 - 0.185x + 3.233x^2 - 8.38x^3 + 9.41x^4 - 5x^5 + 1x^6 \quad (7)$$

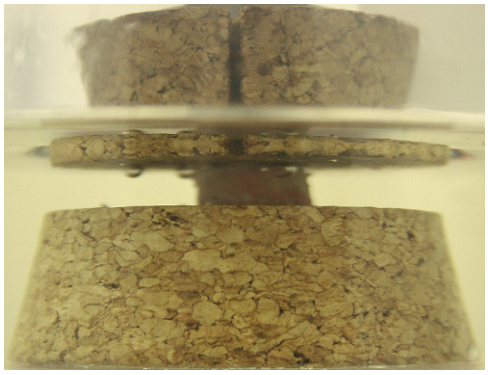

Fig. 13. Articular Cartilage in the test chamber

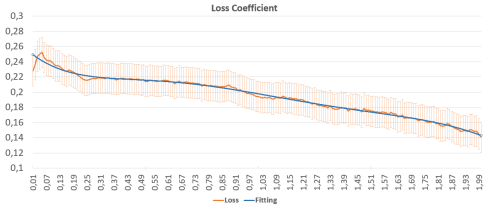

Fig. 14. Frequency-Loss coefficient graph

The loss coefficient determined by tan(δ) has a negative variation (Fig. 12); the fitting has as equation:

$$f(x) = 0.63 - 4.839x + 15.164x^2 - 24.455x^3 + 21.245x^4 - 9.465x^5 + 1.695x^6 \quad (8)$$

Despite the silicone samples had different curing times and small physical differences, tests produced similar results, highlighting the reliability of the rheometer in the predetermined range. Having been checked for good reliability of the device, the dynamic characteristics of hyaline or joint cartilage samples were evaluated. The specimens used in tests were extracted from a cow's knee joint, in particular from the bottom part of the femur. The specimens were fresh when were used and had characteristics:

- 1 mm of cartilage attached to 5 mm of subchondral bone;
- 1 mm of cartilage attached to 1 mm of subchondral bone.

To begin the test, the specimen is inserted into the test chamber full of saline solution (Fig. 13), needed to simulate the real condition into the knee joint. The range of frequencies used in tests was $0.01 \div 2$ Hz. The cartilage was compressed with a force of about 0.7N and left to relax for about 300 s prior to imposing the γ angular deformation. The results were satisfactory as comparable with those of the literature. The graphs of complex module (Fig. 15) and loss coefficient (Fig. 14) as a result of a test. The graphs founded in literature (Fig. 16) are similar to the graphs that the CS made, so this confirm that the Software do his job very well. The complex modulus is measured in MPa and the frequency in Hz. A sixth order equations of the complex modulus and of the loss coefficient

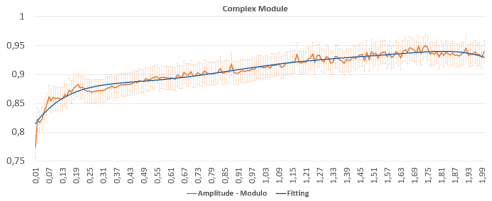

Fig. 15. Frequency-Complex modulus graph

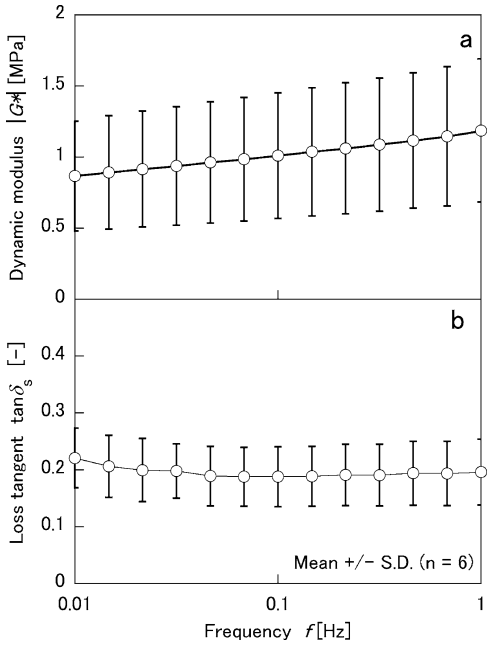

Fig. 16. Literature plots

were extracted from the data processed by software:

$$y = -1E - 13x^6 + 8E - 11x^5 - 2E - 08x^4 + 3E - 06x^3 - 0,0002x^2 + 0,0055x + 0,8096 \quad (9)$$

$$y = 2E - 14x^6 - 2E - 11x^5 + 6E - 09x^4 + 9E - 07x^3 + 6E - 05x^2 - 0,0024x + 0,2518 \quad (10)$$

the 9 is the equation that rappresents the fitting curve of the complex modulus, the 10 is the fitting's equation of the loss coefficient. This test aims to demonstrate that the energy applied to the AC gives a response that changes, from a prevalently viscous behaviour to a prevalently elastic behaviour with the increase of frequency of application of the oscillations.

V. Conclusion

The predetermined objective in this work was the design and realization of a software able to control an instrument, the rheometer, for evaluate the viscoelastic properties of cartilage or more generally of two-phase materials. The instrument made has proved able to meet the expectations, providing results consistent with those reported in the literature. The developed software allows complete control with regard to the action on the specimen and the analysis of its reactions,

thus making it completely self-sufficient machine. In fact the use of advanced soft computing techniques has became progressively an effective option in many contexts [**?**], [19]–[24]. It was created a campaign of tests, both of elastomers that of biological tissues, which allowed to calibrate the machine both from a hardware and software point of view and to verify the results which, as mentioned, are consistent with those found in the literature.

REFERENCES

[1] M. Calì and F. Lo Savio, "Accurate 3d reconstruction of a rubber membrane inflated during a bulge test to evaluate anisotropy," in *Advances on Mechanics, Design Engineering and Manufacturing*. Springer International Publishing, 2017, pp. 1221–1231.

[2] K. Boettcher, S. Grumbein, U. Winkler, J. Nachtsheim, and O. Lieleg, "Adapting a commercial shear rheometer for applications in cartilage research," *Review of Scientific Instruments*, vol. 85, no. 9, p. 093903, 2014.

[3] M. R. VanLandingham, N.-K. Chang, P. Drzal, C. C. White, and S.-H. Chang, "Viscoelastic characterization of polymers using instrumented indentation. i. quasi-static testing," *Journal of Polymer Science Part B: Polymer Physics*, vol. 43, no. 14, pp. 1794–1811, 2005.

[4] M. Calì, D. Speranza, and M. Martorelli, "Dynamic spinnaker performance through digital photogrammetry, numerical analysis and experimental tests," in *Advances on Mechanics, Design Engineering and Manufacturing*. Springer, 2017, pp. 585–595.

[5] V. C. Mow, S. Kuei, W. M. Lai, and C. G. Armstrong, "Biphasic creep and stress relaxation of articular cartilage in compression: theory and experiments," *Journal of biomechanical engineering*, vol. 102, no. 1, pp. 73–84, 1980.

[6] S. Miyata, T. Tateishi, K. Furukawa, and T. Ushida, "Influence of structure and composition on dynamic viscoelastic property of cartilaginous tissue: criteria for classification between hyaline cartilage and fibrocartilage based on mechanical function," *JSME International Journal Series C Mechanical Systems, Machine Elements and Manufacturing*, vol. 48, no. 4, pp. 547–554, 2005.

[7] A. Mak, "The apparent viscoelastic behavior of articular cartilagethe contributions from the intrinsic matrix viscoelasticity and interstitial fluid flows," *Journal of biomechanical engineering*, vol. 108, no. 2, pp. 123–130, 1986.

[8] M. Stading and R. Langer, "Mechanical shear properties of cell-polymer cartilage constructs," *Tissue engineering*, vol. 5, no. 3, pp. 241–250, 1999.

[9] S. C. R. Skalak, *Handbook of Bioengineering*. McGraw Hill, 1986, ch. 4.

[10] L. Q. Wan, J. Jiang, D. E. Miller, X. E. Guo, V. C. Mow, and H. H. Lu, "Matrix deposition modulates the viscoelastic shear properties of hydrogel-based cartilage grafts," *Tissue Engineering Part A*, vol. 17, no. 7-8, pp. 1111–1122, 2011.

[11] G. Vunjak-Novakovic and S. Goldstein, "Biomechanical principles of cartilage and bone tissue engineering," *Basic orthopaedic biomechanics and mechanobiology*, pp. 343–408, 2005.

[12] A. A. Spirt, A. F. Mak, and R. P. Wassell, "Nonlinear viscoelastic properties of articular cartilage in shear," *Journal of Orthopaedic Research*, vol. 7, no. 1, pp. 43–49, 1989.

[13] D. A. Grande, A. S. Breitbart, J. Mason, C. Paulino, J. Laser, and R. E. Schwartz, "Cartilage tissue engineering: current limitations and solutions." *Clinical orthopaedics and related research*, vol. 367, pp. S176–S185, 1999.

[14] G. La Rosa, F. Lo Savio, E. Pedullà, and E. Rapisarda, "Developing of a new device for static and dynamic tests of ni-ti instruments for root canal treatment," *Procedia Structural Integrity*, vol. 2, pp. 1303–1310, 2016.

[15] E. Pedullà, F. Lo Savio, S. Boninelli, G. Plotino, N. M. Grande, G. La Rosa, and E. Rapisarda, "Torsional and cyclic fatigue resistance of a new nickel-titanium instrument manufactured by electrical discharge machining," *Journal of endodontics*, vol. 42, no. 1, pp. 156–159, 2016.

[16] G. Sequenzia, S. Oliveri, M. Calabretta, G. Fatuzzo, and M. Cali, "A new methodology for calculating and modelling non-linear springs in the valve train of internal combustion engines," in *SAE Technical Paper*. SAE International, 04 2011.

[17] E. Pedulla, F. Lo Savio, G. Plotino, N. M. Grande, S. Rapisarda, G. Gambarini, and G. La Rosa, "Effect of cyclic torsional preloading on cyclic fatigue resistance of protaper next and mtwo nickel–titanium instruments," *Giornale Italiano di Endodonzia*, vol. 29, no. 1, pp. 3–8, 2015.

[18] F. Lo Savio, E. Pedullà, E. Rapisarda, and G. La Rosa, "Influence of heat-treatment on torsional resistance to fracture of nickel-titanium endodontic instruments," *Procedia Structural Integrity*, vol. 2, pp. 1311–1318, 2016.

[19] M. Wozniak, C. Napoli, E. Tramontana, and G. Capizzi, "A multiscale image compressor with rbfnn and discrete wavelet decomposition," in *International Joint Conference on Neural Networks (IJCNN)*. IEEE, 2015, pp. 1219–1225.

[20] G. Capizzi, G. Lo Sciuto, C. Napoli, and E. Tramontana, "A multithread nested neural network architecture to model surface plasmon polaritons propagation," *Micromachines*, vol. 7, no. 7, p. 110, 2016. [Online]. Available: http://www.mdpi.com/2072-666X/7/7/110

[21] C. Napoli and E. Tramontana, "Massively parallel wrnn reconstructors for spectrum recovery in astronomical photometrical surveys," *Neural Networks*, vol. 83, pp. 42–50.

[22] C. Napoli, G. Pappalardo, M. Tina, and E. Tramontana, "Cooperative strategy for optimal management of smart grids by wavelet rnns and cloud computing," *IEEE Transactions on Neural Networks and Learning Systems*, vol. 27, no. 8, pp. 1672–1685, 2016.

[23] F. Bonanno, G. Capizzi, and G. Lo Sciuto, "A neuro wavelet-based approach for short-term load forecasting in integrated generation systems," in *Clean Electrical Power (ICCEP), 2013 International Conference on*. IEEE, 2013, pp. 772–776.

[24] F. Bonanno, G. Capizzi, S. Coco, A. Laudani, and G. Lo Sciuto, "A coupled design optimization methodology for li-ion batteries in electric vehicle applications based on fem and neural networks," in *Power Electronics, Electrical Drives, Automation and Motion (SPEEDAM), 2014 International Symposium on*. IEEE, 2014, pp. 146–153.

[25] D. Gotleyb, G. Lo Sciuto, C. Napoli, R. Shikler, E. Tramontana, and M. Woźniak, "Characterisation and modeling of organic solar cells by using radial basis neural networks," in *International Conference on Artificial Intelligence and Soft Computing*. Springer, 2016, pp. 91–103.